6th March 2012

Long-lived staus from strong production in a simplified model approach

Jan Heisig and Jörn Kersten

II. Institute for Theoretical Physics, University of Hamburg, Germany

jan.heisig@desy.de, joern.kersten@desy.de

Abstract

We study the phenomenology of a supersymmetric scenario where the next-to-lightest superparticle is the lighter stau and is long-lived due to a very weakly coupled lightest superparticle, such as the gravitino. We investigate the LHC sensitivity and its dependence on the superparticle spectrum with an emphasis on strong production and decay. We do not assume any high-scale model for SUSY breaking but work along the lines of simplified models. Devising cuts that yield a large detection efficiency in the whole parameter space, we determine the LHC's discovery and exclusion potential. This allows us to derive robust limits on $m_{\widetilde{\tau}_1}$, $m_{\widetilde{g}}$, a common $m_{\widetilde{q}}$, and $m_{\widetilde{t}_1}$. We briefly discuss the prospects for observing stopped staus.

Contents

1 Introduction

In supersymmetric scenarios where the gravitino is the lightest superparticle (LSP), the decay of the next-to-LSP (NLSP) is suppressed by the very weak gravitino interactions, as long as R parity is conserved. For a gravitino mass above a few keV, NLSPs produced at a collider usually have a decay length that is large compared to the size of the detector. The same is possible in axino LSP scenarios. For a charged NLSP such as a stau, this leads to the exciting possibility of finding SUSY in events with no missing energy and two charged tracks leaving the detector.

In a collider experiment such a long-lived stau can either be produced directly or in a decay chain following the initial production of a pair of superparticles. At the LHC the production of the strongly interacting squarks and gluinos clearly has the biggest potential to dominate over other production mechanisms. This is why in this work we concentrate on the strong production. Unfortunately, a considerable part of the more than 100 free parameters of the MSSM influences the signature of staus via the appearance of intermediate sparticles in the cascades. This general problem of the large SUSY parameter space has often been tackled by studying constrained models such as the CMSSM. The nonobservation of SUSY has severely reduced the constrained model parameter space. Among other things, this has driven the interest in model-independent studies, including regions in parameter space that are not covered by constrained models.

There are basically two ways of going beyond constrained models. The first is to use a well-motivated set of 19 free parameters in the framework of the phenomenological MSSM [1] and perform a Monte Carlo scan over the (still vast) parameter space, displaying the behavior of observables in a scatter plot (see e.g. [2]). The second is to reduce the parameter space in a bottom-up approach more drastically after identifying the most important low-scale parameters that determine the signature. This latter approach finds its realization in the so-called simplified models [3, 4]. So far the idea of simplified models has not been considered in the case of a very weakly interacting LSP. Nonetheless, it is especially suitable in the case of a long-lived stau scenario, as we will show in this paper.

We will determine the LHC sensitivity for a general long-lived stau[1] scenario utilizing a simplified-model approach. We consider the 8 TeV and the 14 TeV LHC runs. If not stated otherwise, we refer to the 8 TeV run. We consider the particles of the MSSM as the only particles involved in the interactions inside the collider. We shall assume that there is no accidental phase space suppression that renders any sparticle other than the stau NLSP long-lived.

We will define a set of simplified models in section 2. We will divide the problem into two parts—the production and the decay. We will first discuss how the production cross section depends on the mass pattern in the squark and gluino sector. This discussion is general and applies to any LSP scenario. However, we will consider a range of sparticle masses around the LHC limits that are typically reachable in the long-lived stau scenario. Our results will be presented for the two limiting cases of a common squark mass and of a scenario in which one of the stops is much lighter than all other squarks. In each case we will allow for two free parameters: the gluino mass and either the common squark mass or the stop mass. We will then consider the decay of colored sparticles into the stau NLSP and discuss the impact of the intermediate sparticles in the decay chain on the observables. This discussion is based on the observation that the direct signature of the stau (rather than SM particles from the cascade) provides the most significant contribution to a potential discovery or an exclusion. Since the identifiability of the stau depends strongly on its velocity, our considerations are driven by the quest of finding the quantities the stau velocity dominantly depends on. This necessitates introducing the stau mass as the third free parameter. We will define three simplified models that serve as limiting cases and thus are able to capture the phenomenology of any realistic spectrum within the long-lived stau scenario.

In section 3 we will study the relevant background sources and discuss the rejection obtained by a cut on the velocity of a stau candidate. Due to two distinct measurements of the velocity and the requirement of two staus per event, an excellent background rejection is possible. For certain regions in parameter space a large number of staus are likely to be missed by the current trigger settings. Hence, we will propose a dedicated trigger in order to be able to record the corresponding events. In section 3.4 we will introduce selection criteria that achieve high efficiencies in the whole parameter space.

In section 4 we will present the results obtained in a Monte Carlo study by scanning over the defined parameter space. We will show the discovery and exclusion reach in

[1]The analysis is virtually identical for any charged slepton NLSP.

terms of the stau, squark and gluino masses, both with and without utilizing the proposed trigger setup. These results represent conservative, model-independent bounds and thus can be applied to all models with a long-lived charged slepton.

Some staus may be stopped inside the detector and decay much later. We will discuss the potential for observing such decays in section 5, estimating the number of staus that are available for the analysis.

2 Simplified models for long-lived stau scenarios

The task of simplified models is to reduce the huge SUSY parameter space. The same is true for constrained models, but those obtain a reduction by imposing boundary conditions with few parameters at a very high energy scale. In simplified models the reduction is driven by the signatures at colliders. We aim to determine the most important low-energy parameters governing the LHC sensitivity to long-lived staus originating from cascades following the strong production of SUSY particles.

2.1 Production

Obviously, the masses of the produced squarks and gluinos play an important role—the production cross section depends on them. The first simplifying assumption we discuss is a common mass for all squarks. In the high-mass region, which we are primarily interested in, the production of squarks requires partons with a large momentum fraction. The corresponding parton distribution functions (PDFs) of u and d quarks are much larger than those of heavier quarks and of antiquarks. Hence, governed by the large contribution of the first-generation squarks, $\widetilde{q}\widetilde{q}$ production dominates over $\widetilde{q}\overline{\widetilde{q}}$ (see upper right panel of figure 8), and $\widetilde{g}\widetilde{q}$ dominates over $\widetilde{g}\overline{\widetilde{q}}$. The latter is even negligible and thus not considered here at all.

The effects of abandoning the assumption of a common squark mass are displayed in figure 1. The left panel shows the next-to-leading order (NLO) cross section for $\widetilde{q}\widetilde{q}$ production computed by PROSPINO 2 [5] as a function of $m_{\widetilde{d}}$ (red dashed curve originating at 1 on the ordinate), $m_{\widetilde{u}}$ (green solid curve) and $m_{\widetilde{u},\,\widetilde{d}} = m_{\widetilde{d}} = m_{\widetilde{u}}$ (blue dotted curve). In each case, all other squark masses are degenerate at $m_{\widetilde{q}} = 1600\,\text{GeV}$. We normalized the curves to the $\widetilde{q}\widetilde{q}$ production cross section at the point where *all* squarks are mass degenerate. The ratio $m_{\widetilde{g}}/m_{\widetilde{q}}$ is chosen to be 1.68. This is the value where $\widetilde{q}\widetilde{q}$ production contributes maximally to the total cross section of colored sparticles in figure 8. From figure 1 it is obvious that the contribution of the first-generation squarks is dominant—in the case where $\widetilde{d}$ and $\widetilde{u}$ masses increase simultaneously, the $\widetilde{q}\widetilde{q}$ cross section drops drastically. Decoupling either only $\widetilde{u}$ or only $\widetilde{d}$ has a much less drastic effect. Decoupling the squarks other than $\widetilde{u}$ and $\widetilde{d}$ does not significantly change the production cross section. Additionally, we plot the analogous curves for $\widetilde{q}\overline{\widetilde{q}}$ production (curves originating at slightly above 0.1 on the ordinate). Here, the t-channel contribution, which introduces the flavor dependence, is much less important. Consequently, if we decouple both $\widetilde{d}$ and $\widetilde{u}$, the $\widetilde{q}\overline{\widetilde{q}}$ cross section drops much more moderately than the one for $\widetilde{q}\widetilde{q}$ and hence becomes

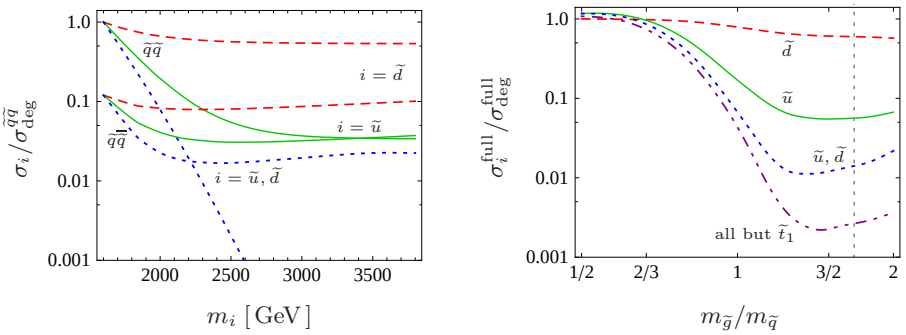

Figure 1: NLO cross sections for the production of colored sparticles at the 8 TeV LHC. *Left:* Squark-squark (curves originating at 1 on the ordinate) and squark-antisquark production (curves originating below) as a function of the mass m_i of different squark species. All other squark masses are degenerate at $m_{\widetilde{q}} = 1600\,\text{GeV}$ and $m_{\widetilde{g}}/m_{\widetilde{q}} \simeq 1.68$. The curves are normalized to the squark-squark production cross section for the fully degenerate case, i.e., $m_i = m_{\widetilde{q}}$. *Right:* Total cross section for all production channels (normalized to the cross section with degenerate masses) along a typical LHC sensitivity limit (see figure 8) parametrized by the ratio $m_{\widetilde{g}}/m_{\widetilde{q}}$. We decoupled $\widetilde{d}$, $\widetilde{u}$, and both flavors, obtaining the red dashed, green solid, and blue dotted lines, respectively. The purple dot-dot-dashed curve shows the cross section for $\widetilde{q} = \widetilde{t}_1$ and all other squarks decoupled.

dominant. As we stated above, $\widetilde{g}\overline{\widetilde{q}}$ is negligible compared to the other contributions, and so is $\widetilde{g}\widetilde{q}$ in the case of decoupled $\widetilde{u}$ and $\widetilde{d}$—the cross section drops by two orders of magnitude. Consequently, for decoupled first-generation squarks, $\widetilde{q}\overline{\widetilde{q}}$ and $\widetilde{g}\widetilde{g}$ remain the most important production channels. The latter channel is evidently much less sensitive to the squark masses.

In the right panel of figure 1 we plot the total cross section for all production channels ($\widetilde{g}\widetilde{g}$, $\widetilde{g}\widetilde{q}$, $\widetilde{q}\widetilde{q}$, $\widetilde{q}\overline{\widetilde{q}}$) along an expected 8 TeV LHC sensitivity limit (black dashed line in the left panel of figure 8) parametrized by the ratio $m_{\widetilde{g}}/m_{\widetilde{q}}$. As before, different squark species are decoupled while the remaining squarks have a common mass $m_{\widetilde{q}}$, and for each value of $m_{\widetilde{g}}/m_{\widetilde{q}}$ the cross section is normalized to the cross section with degenerate squark masses. The vertical dotted line marks the ratio $m_{\widetilde{g}}/m_{\widetilde{q}} \simeq 1.68$ used in the left panel. Stop production is not included in the curves corresponding to decoupling $\widetilde{d}$ or $\widetilde{u}$. However, it would change only the blue dotted curve noticeably, giving an enhancement by a factor 4/3. In each case considered so far, the right- and left-handed squarks were treated uniformly. Since the strong interaction is not chiral, decoupling only $\widetilde{q}_{\rm L}$ or $\widetilde{q}_{\rm R}$ merely results in a combinatorial factor that does not involve information from the PDFs.

The lowermost curve in the right panel of figure 1 corresponds to decoupling all squarks but the lighter stop. Decoupling all squarks except either $\widetilde{t}_2$ or one $\widetilde{b}$, $\widetilde{c}$ or $\widetilde{s}$ squark would give the same result. This scenario provides the limiting case of a minimal cross section.

We are left with two limiting setups, the one with a common squark mass and the light stop scenario. Each contains two free parameters, $m_{\widetilde{g}}$ and $m_{\widetilde{q}}$, or $m_{\widetilde{g}}$ and $m_{\widetilde{t}_1}$, respectively. We will focus on the former case but come back to the latter scenario in section 4.3. From the discussion in this section the LHC reach for a general scenario can

be estimated.

2.2 Decay

After the production of squarks and gluinos, these particles decay via a cascade to the stau NLSP. The mass difference between the lightest colored sparticle (LCP) and the stau NLSP determines the total phase space available in the cascade. Thus, it strongly affects the kinematics of the stau (and of the SM particle radiation). We will therefore consider as a third free parameter the stau mass.

In order to study the impact of the intermediate sparticles in the cascade, we consider limiting cases. Following the considerations in [6, 7] and translating them into the stau NLSP scenario we find that within the MSSM there are no spectra for which the LCP preferably decays via chains containing more than three intermediate sparticles between the LCP and NLSP. In large regions of the parameter space, shorter decay chains give the dominant contribution.

We focus on the impact of the mass spectrum on the stau velocity, which is the most important quantity affecting the identification of staus. We consider the limit where only massless SM particles are produced in the cascade. For a two-body decay the velocity of the daughter sparticle $i+1$ in the rest frame of the mother sparticle i is

$$\beta_{i+1}^{(i)} = \frac{m_i^2 - m_{i+1}^2}{m_i^2 + m_{i+1}^2}\,. \tag{1}$$

If the mother sparticle has velocity β_i in the lab frame, the velocity of the daughter sparticle in the lab frame reads

$$\beta_{i+1} = \sqrt{1 - \frac{(1-\beta_i^2)\big(1-{\beta_{i+1}^{(i)}}^2\big)}{\big(1+\beta_i\,\beta_{i+1}^{(i)}\cos\theta_{i+1}^{(i)}\big)^2}}\,, \tag{2}$$

where $\theta_{i+1}^{(i)}$ is the decay angle in the rest frame of the mother sparticle. Assuming a fixed mass gap $m_0 - m_n$ ($= m_{\rm LCP} - m_{\widetilde{\tau}_1}$) and considering an $(n-1)$-step decay[2] ($m_0 \geq m_1 \geq \cdots \geq m_n$) with a uniform probability distribution for $\theta_{i+1}^{(i)}$ in each decay (i.e., ignoring spin correlations), we can compute the mean of the NLSP velocity β_n as a function of all masses and the LCP velocity β_0,

$$\overline{\beta}_n = \overline{\beta}_n(\beta_0, m_1, \ldots, m_{n-1})\,. \tag{3}$$

It turns out that $\overline{\beta}_n$ has one minimum (maximum) at the point given by the mass pattern[3]

$$m_i \simeq m_0^{\frac{n-i}{n}}\, m_n^{\frac{i}{n}} \tag{4}$$

[2]Following [4], we refer to a cascade with n intermediate sparticles between the LCP and the NLSP as an 'n-step decay'. For instance, the decay $\widetilde{q} \to \widetilde{\chi}^0 \to \widetilde{\tau}$ is a 1-step decay.

[3]We checked this explicitly up to $n = 3$ but expect it to hold for any n.

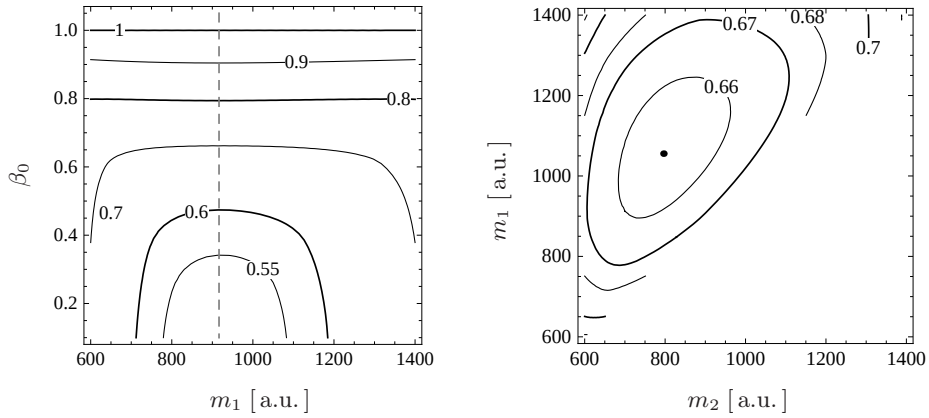

Figure 2: Contours of constant average velocity $\overline{\beta}_n(\beta_0, m_1, \ldots, m_{n-1})$ for $m_0 = 1400$ and $m_n = 600$ in arbitrary units. (The overall mass scale is irrelevant. For convenience we chose values that could be realistic masses in GeV.) *Left:* $\overline{\beta}_2$ as a function of β_0 and m_1. The dashed vertical line denotes the extremum according to (4). For $\beta_0 \lesssim 0.77$ it is a minimum. Above this value it turns into a maximum, which is not very pronounced, though, as $\overline{\beta}_2$ is nearly independent of m_1. *Right:* $\overline{\beta}_3$ as a function of m_1 and m_2 for $\beta_0 = 0.6$. The central dot denotes the minimum according to (4). The maxima according to (5) are located in the lower-left, upper-left and upper-right corners. The limiting case of an effective 1-step decay chain ($n = 2$) lies on the borders of the contour plot—the upper border ($m_1 = m_0$), the left border ($m_2 = m_3$) and the diagonal ($m_1 = m_2$).

and n maxima (minima) at

$$m_i = m_0\,, \quad m_j = m_n \quad \forall\, i < k,\ j \geq k\,, \quad k = 1, \ldots, n\,. \tag{5}$$

The extrema (5) represent the mass-degenerate limit and correspond (in the approximation we are currently working in) to the direct decay of the LCP into the NLSP. The result (4) is not surprising: it renders all velocities $\beta_{i+1}^{(i)}$ to be equal—on average each decay gives the same contribution to the velocity of the NLSP. In contrast, in (5) one decay dominates over the others. The result also implies that the extremal values of $\overline{\beta}_m$ lie between those of $\overline{\beta}_n$ if $m < n$. The m-step decays represent a slice in the space of the masses in the n-step decays with $n - m$ masses degenerate. This slice clearly does not contain the point (4).

Whether (4) is a minimum or a maximum depends on β_0. In fact, (4) is a maximum only if β_0 is very close to the speed of light (see the left panel of figure 2). The high efficiency obtained in the long-lived stau search (see section 3.4) pushes the boundaries of the LHC sensitivity to high squark and gluino masses. Hence, they will typically be produced rather close to threshold and thus β_0 is expected to be significantly below 1, at least if LCP production dominates. In this case (4) is a minimum of $\overline{\beta}_n$. The right panel of figure 2 shows the contours in $\overline{\beta}_3$ for a 2-step decay as a function of m_1 and m_2.

We can now formulate appropriate simplified models. We see that the direct decay of the LCP into the stau mediated by a nearly mass-degenerate neutralino as well as the mass pattern (4) are reasonable benchmark mass patterns. We will display our results

for three choices.

Model $\mathcal{A}$ The 'direct decay' via a nearly degenerate neutralino ($m_{\widetilde{\chi}^0} \simeq m_{\widetilde{\tau}_1}$).

Model $\mathcal{B}$ The mass pattern (4) for the 1-step decay LCP $\to \widetilde{\chi}^0 \to \widetilde{\tau}$, $m_{\widetilde{\chi}^0} = \sqrt{m_{\mathrm{LCP}} m_{\widetilde{\tau}_1}}$.

Model $\mathcal{C}$ The mass pattern (4) for the 3-step decay LCP $\to \widetilde{\chi}_2^0 \to \widetilde{\ell} \to \widetilde{\chi}_1^0 \to \widetilde{\tau}$.

In all cases we will force the respective branching ratios to provide the desired cascades (see section 4.1 for details). We will assume symmetric decay chains, i.e., the same cascade for both LCPs produced in an event. We will briefly discuss the issue of asymmetric chains in section 4.2.

The model with pattern (4) and the 2-step decay LCP $\to \widetilde{\chi}_2^0 \to \widetilde{\chi}_1^0 \to \widetilde{\tau}$ turned out to lie completely between $\mathcal{B}$ and $\mathcal{C}$ concerning the LHC sensitivity shown in section 4.2. By this we implicitly checked also that the appearance of the heavy SM particle radiated in the decay of the heavier neutralino does not change the qualitative picture. Threshold effects are expected to be small due to the large SUSY masses.[4]

3 Background estimation and selection criteria

For the initial production of colored superparticles, each event contains at least two jets, two staus and two taus or tau neutrinos. As the identification of taus it not very efficient, we do not include them in the signature. Furthermore, we will see that the background rejection can already be saturated with staus and jets alone.

In the detector, long-lived staus show up as muon-like particles, i.e., charged particles usually leaving the detector. They can have a velocity β significantly below the speed of light, which allows one to distinguish them from muons by virtue of a cut on β. However, in some regions in parameter space many staus are produced with a velocity close to 1. These regions typically feature spectra with large mass gaps $m_{\mathrm{LCP}} - m_{\widetilde{\tau}_1}$. Requiring hard jets can alleviate the drop in sensitivity when β approaches 1, allowing a relaxation of the cut on β. However, dropping the β cut completely will lead to a substantial loss of sensitivity due to a dramatic increase of the (then unsuppressed) muon background.[5] Thus, we will always require identified staus. If the staus stem from rather compressed spectra the jets are expected to be soft. On the other hand, the staus tend to be slow in these cases, so identified staus alone suffice for a good sensitivity.

Since the SUSY particles are always produced in pairs, the largest significance can be achieved by requiring *two* stau candidates in each event. Therefore, we use the following signature for SUSY events:

[4] An exception could be a dominant decay chain with Higgsinos whose decay produces a heavy Higgs. Here, threshold effects can be somewhat more important but are not expected to change the picture significantly.

[5] A sufficient background rejection might be achievable without a velocity discrimination if a very specific signature of SM radiation is considered. However, such a search would introduce a strong model dependence, which is against the idea of this work.

- 2 high-p_{T}, isolated muon-like particles passing a velocity cut and
- (optionally) 2 high-p_{T} jets.

3.1 Background kinematics

As background we consider all relevant SM processes providing two (isolated) muons. We will examine the behavior under several kinematic cuts in this subsection. In the next subsection we will discuss how the background is further reduced by a cut on the velocity.

We consider the Drell-Yan (DY) production of muons ($Z/\gamma \to \mu\mu$) and taus ($Z/\gamma \to \tau\tau$), di-boson production (W^+W^-, WZ and ZZ), $t\bar{t}$ production, single t production (tW plus tb) and associated Wb production, with jets from initial or final state radiation. We calculated the cross section for DY production with FEWZ [8] at next-to-NLO (NNLO) accuracy. The cross sections for di-boson production [9], $t\bar{t}$ and single t production [10, 11] as well as associated Wb production [12, 13] were calculated via MCFM [14] at NLO precision. We generated the events with MadEvent 5 [15]. To regularize the collinear singularity and gain generator efficiency we imposed the generator-level cuts $p_{\mathrm{T}}^{\ell} > 60\,\mathrm{GeV}$ (on both leptons) and $p_{\mathrm{T}}^{b} > 60\,\mathrm{GeV}$ (required for at least one b quark) in the normalization and event generation of the processes DY and Wb, respectively. The resulting cross sections are summarized in table 1.

We performed showering and hadronization with Pythia 6 [16]. Since we will impose a selection criterion requiring two hard jets, the distribution of the two leading jets should be reliable up to very high p_{T}. Therefore, for the processes DY, W^+W^-, single t and Wb we include up to two additional jets in the matrix element simulation of MadEvent, whereas for the processes WZ, ZZ[6] and $t\bar{t}$ we consider up to one additional jet—in the latter processes (at least) one of the two leading jets is expected to originate from the decay of a heavy SM particle. In the case of Wb, one of the additional jets in the matrix element is allowed to be a b jet in order to include the $Wb\bar{b}$ contribution. In order to properly match the different contributions to the inclusive sample, which contains jets both from showering and from the matrix element, we applied the MLM matching procedure [17] and chose `xqcut` $= p_{\mathrm{T}}^{\mathrm{jet,\,min}} = 30\,\mathrm{GeV}$ and `QCUT` $= 40\,\mathrm{GeV}$. We used the Cteq6l1 PDF set [18].

We passed the output of Pythia to the detector simulation Delphes 1.9 [19] and applied a cut and count analysis on the lhco output of Delphes. The reconstruction efficiency for each muon was set to 0.9. The trigger efficiency was conservatively set to 100% for the background. Figure 3 shows the cross sections for all considered background processes as functions of various cuts on characteristic variables. These variables are the transverse momentum of the muon p_{T}^{μ} and of the jet $p_{\mathrm{T}}^{\mathrm{jet}}$, the difference of the p_{T} of the

[6] If both of the two hardest jets did not originate from the W or Z, respectively, but from initial state radiation, this process would be just another correction to the DY process with an additional suppression by the weak coupling due to the production of the extra vector boson. Hence, we can easily estimate that such a process cannot compete with the DY process, independent of the cuts we apply on the two jets and muons.

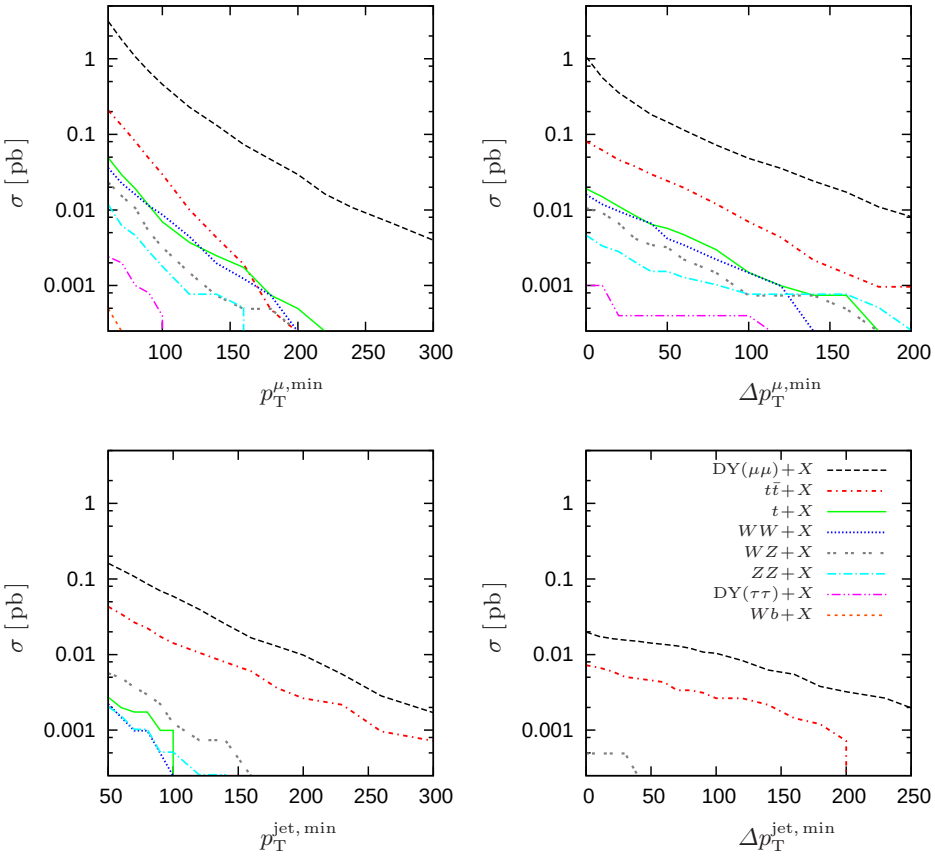

Figure 3: Inclusive cross section of the considered SM background processes as a function of various cuts at the 8 TeV LHC. In all plots we imposed the isolation cut $I_{\mathrm{rel}} < 0.2$ and the pseudorapidity cut $|\eta| < 2.4$ on each muon. *Top left:* Requiring at least two muons with $p_{\mathrm{T}}^{\mu} > p_{\mathrm{T}}^{\mu,\mathrm{min}}$ each. $p_{\mathrm{T}}^{\mu,\mathrm{min}}$ is varied. *Top right:* Requiring at least two muons with $p_{\mathrm{T}}^{\mu} > 80\,\mathrm{GeV}$ and $\Delta p_{\mathrm{T}}^{\mu} > \Delta p_{\mathrm{T}}^{\mu,\mathrm{min}}$. $\Delta p_{\mathrm{T}}^{\mu,\mathrm{min}}$ is varied. *Bottom left:* Requiring at least two muons with $p_{\mathrm{T}}^{\mu} > 80\,\mathrm{GeV}$ and additionally at least two jets with $p_{\mathrm{T}}^{\mathrm{jet}} > p_{\mathrm{T}}^{\mathrm{jet,\,min}}$ each. We vary $p_{\mathrm{T}}^{\mathrm{jet,\,min}}$. *Bottom right:* Requiring at least two muons with $p_{\mathrm{T}}^{\mu} > 80\,\mathrm{GeV}$ and additionally at least two jets with $p_{\mathrm{T}}^{\mathrm{jet}} > 150\,\mathrm{GeV}$ each as well as $\Delta p_{\mathrm{T}}^{\mathrm{jet}} > \Delta p_{\mathrm{T}}^{\mathrm{jet,\,min}}$. We vary $\Delta p_{\mathrm{T}}^{\mathrm{jet,\,min}}$. The key in the bottom right panel holds for all panels.

		σ [pb]			
process	order	total	selection 1	selection 2	selection 3
DY($\mu\mu$)+X	NNLO	5.53	0.0038	0.0971	0.0040
DY($\tau\tau$)+X	NNLO	5.53	<0.0002	<0.0002	<0.0002
W^+W^-+X	NLO	57.3	<0.0002	0.0015	0.0002
$WZ+X$	NLO	22.8	<0.0002	0.0005	<0.0002
$ZZ+X$	NLO	7.92	<0.0002	0.0005	<0.0002
$t\bar{t}+X$	NLO	256	0.0019	0.0034	<0.0002
$t+X$	NLO	96.5	<0.0002	0.0022	<0.0002
$Wb+X$	NLO	36.2	<0.0002	<0.0002	<0.0002
Σ | before β-cuts			0.0069	0.1055	0.0054
Σ | after β-cuts			4.8×10^{-7}	8.2×10^{-8}	$< 10^{-9}$

Table 1: Cross sections for the considered background sources at the 8 TeV LHC. We display the total cross sections as computed at the given precision (see text for details) as well as the cross sections times efficiency obtained by applying the cuts selection criteria 1–3 defined in section 3.4 but without cuts on the velocity β. The cuts on the velocity belonging to selection criteria 1–3 are only applied in the very last line.

two considered muons,

$$\Delta p_{\mathrm{T}}^{\mu} = |p_{\mathrm{T}}^{\mu,1} - p_{\mathrm{T}}^{\mu,2}|\,, \tag{6}$$

and of the two considered (hardest) jets,

$$\Delta p_{\mathrm{T}}^{\mathrm{jet}} = |p_{\mathrm{T}}^{\mathrm{jet},1} - p_{\mathrm{T}}^{\mathrm{jet},2}|\,. \tag{7}$$

To reject the QCD background we require *isolated* muons, i.e., $I_{\mathrm{rel}} < I_{\mathrm{rel}}^{\mathrm{max}}$, where

$$I_{\mathrm{rel}} = \frac{\sum_{i\neq\mu} p_{\mathrm{T},i}^{\mathrm{track}} + \sum_{i\neq\mu} E_{\mathrm{T},i}^{\mathrm{CAL}}}{p_{\mathrm{T}}^{\mu}} \tag{8}$$

is the relative isolation. In (8) the sums are performed over all objects within a cone of a given $\Delta R \equiv \sqrt{\Delta\eta^2 + \Delta\phi^2} = 0.3$ around the muon.[7]

Except for the $Wb+X$ contribution the background is not sensitive to the precise choice of $I_{\mathrm{rel}}^{\mathrm{max}}$ in a range from 0.02 to 1. The same is true for the typical signal we will consider. In contrast, $Wb + X$ drops significantly with smaller $I_{\mathrm{rel}}^{\mathrm{max}}$ and is practically irrelevant for the chosen value of $I_{\mathrm{rel}}^{\mathrm{max}} = 0.2$. Hard muons originating from $b\bar{b}$ are suppressed even more strongly by the isolation cut and do not play any role here. The same is expected for other QCD backgrounds.

The DY production is the dominant background providing two hard isolated muons even with the requirement of two hard jets. Without the requirement of hard jets, $t\bar{t}+X$ contributes a few percent of the background, while with this requirement its contribution constitutes up to approximately 15%. The other sources are small and do not exceed a few percent in total.

[7]The energy deposition and track associated with this particle itself are excluded from the sums. Throughout this work we use the anti-k_{t} jet clustering algorithm [20].

3.2 Discrimination via the velocity

The main difference between staus and muons is their velocity, which can be measured independently via the ionization loss in the tracker ($\mathrm{d}E/\mathrm{d}x$) and via a time-of-flight (ToF) measurement. The relative uncertainty of the ToF measurement of muons (with $\beta \simeq 1$) is approximately 0.048 in the ATLAS detector [21] and around 0.06 at CMS [22]. The relative uncertainty of the velocity measurement via ionization loss is smaller, around 0.035, but it is biased due to truncation effects [23]. However, in general it will be possible to correct for this bias in an event-by-event analysis. The combination of the ToF and ionization loss measurement [22, 24] yields an unambiguous and very robust measurement of the velocity. Hence, we refer to this combination whenever possible. We estimated the relative uncertainty of the combined measurement by taking the weighted mean of the respective uncertainties for CMS, yielding $\sigma_\beta^{\mathrm{rel}} \simeq 0.032$.

A smearing of the velocity of muons is not included in the detector simulation DELPHES. Assuming that there is no correlation between the velocity mismeasurement and the other observables[8] considered in the previous subsection, we treat the background rejection due to the velocity cut separately from the application of the kinematic cuts discussed there. In other words, for the background we first apply the cuts on I_{rel}, η, $p_{\mathrm{T}}^{\mathrm{jet}}$, p_{T}^{μ} $\Delta p_{\mathrm{T}}^{\mu}$ and $\Delta p_{\mathrm{T}}^{\mathrm{jet}}$ to the generated events and then multiply the resulting cross section by the background rejection factor r_β due to the velocity cut. To estimate r_β we assume a Gaussian smearing of the velocity with the respective width $\sigma_\beta^{\mathrm{rel}}$ given above. In the case of the signal we refrain from smearing the velocity and use the generator-level values (which were passed through DELPHES) to allow for an event-based application of the cuts.

Since we always consider two stau candidates, we can combine the velocities of the two stau candidates in different ways to formulate appropriate cuts, which lead to different factors r_β. In the following, we denote the background rejection factor due to a cut on a *single* muon by $\hat{r}_\beta$. If the velocities of the two staus within one event tend to be correlated, a cut on both stau candidates with the same β_{max} will yield the highest sensitivity. We will denote this cut as

$$\beta^{\square} < \beta_{\mathrm{max}}^{\square}\,. \tag{9}$$

Since the mismeasurement of the velocity of two background muons in one event is not correlated, this yields a background rejection factor of $r_\beta = \hat{r}_\beta^2$. If, in contrast, the velocity of the two staus in one event is strongly uncorrelated, the cut

$$1 - \sqrt{(1-\beta_1)^2 + (1-\beta_2)^2} \equiv \beta^{\circ} < \beta_{\mathrm{max}}^{\circ} \tag{10}$$

yields a higher sensitivity on the signal. The background rejection factor is $r_\beta = \hat{r}_\beta$ in this case (for the considered Gaussian smearing).

[8] This is an obvious assumption for the background muons because a deviation from $\beta = 1$ does not originate from the physical process. A dependence of the velocity measurement on the pseudorapidity was reported to be small [22].

3.3 Lower limits on the velocity

For staus with $\beta < 0.6$ the efficiencies of the current triggers at ATLAS and CMS drop significantly. In order to improve the trigger for very slow staus the tracker data has to be buffered in order to allow for a recording of the tracker data in delay. Very slow staus are typically produced in scenarios with large $m_{\tilde{\tau}_1}$. We therefore propose a recording of up to about four bunch crossings after a trigger by muon-like particles with $p_{\mathrm{T}}^{\mu} > 300\,\mathrm{GeV}$ (500 GeV) at the 8 TeV (14 TeV) LHC run. We do not expect this to cause the recorded event rate to grow significantly. In section 3.4 we will introduce several selection criteria one of which assumes the proposed trigger while the others simply require $\beta > 0.6$.

Although staus suffer a high energy loss due to ionization of the detector material, they will often lose only a small fraction of their total energy. Consequently, their velocity will stay approximately constant when passing the detector. However, since the ionization loss increases with decreasing velocity the ionization loss will become relevant for the kinematics of the stau if the velocity falls below a critical value—staus might then lose their kinetic energy completely and become trapped inside the detector. Since the traveling range of charged particles in matter increases linearly with their mass, heavier staus are more likely to pass the detector than lighter ones with the same velocity. On the other hand, very slow staus typically appear only if they are very heavy, so in conclusion stopped staus are rather the exception than the generic scenario.[9]

However, to be able to record the tracks of the staus we have to make sure that at least one stau reaches the muon chambers to fire the muon trigger.[10] Besides, both have to pass the tracker to allow for an ionization loss measurement. In order to account for this, we used the approximate traveling range of a charged particle in the detector material given in [25] (see section 5 for details) and determined the minimal velocity that still ensures the required traveling range R as a function of the mass of the stau, $\beta_{\mathrm{min}}^{R}(m_{\tilde{\tau}_1})$. The range R was conservatively set to $1200\,\mathrm{g\,cm^{-2}}$ and $12\,000\,\mathrm{g\,cm^{-2}}$ for the requirement of passing the tracker and muon trigger, respectively. For a homogeneous detector material with density $\rho = 8\,\mathrm{g\,cm^{-3}}$, this corresponds to a path length of 1.5 m and 15 m, respectively.

3.4 Selection criteria

We will now introduce a set of three selection criteria, each of which provides strong background rejection and high signal efficiency in its domain in the considered parameter space. The selection criteria are chosen in a complementary way such that the union of these criteria will lead to high efficiencies throughout the whole parameter space of the simplified models introduced in section 2.

In the following, each stau candidate is understood to pass the isolation criterion $I_{\mathrm{rel}} < 0.2$ and to lie within a pseudorapidity range $|\eta| < 2.4$. When we cut on the

[9] We will examine the possibility of observing stopped staus at the LHC in section 5.

[10] This requirement can of course be relaxed if an event contains enough SM particle radiation to fire the trigger.

transverse momentum p_{T}^{2i}, we require *two* particles i that both pass the cut. The values given below are valid for the 8 TeV (14 TeV) LHC analysis. The selection criteria are:

1. Two stau candidates passing the muon chambers,

$$p_{\mathrm{T}}^{2\mu} > 80\,\mathrm{GeV}\ \ (240\,\mathrm{GeV})\,, \quad \Delta p_{\mathrm{T}}^{\mu} > 50\,\mathrm{GeV}\ \ (70\,\mathrm{GeV})\,, \quad \beta^{\circ} < 0.86\,, \tag{11}$$

   and two jets,

$$p_{\mathrm{T}}^{2\mathrm{jet}} > 200\,\mathrm{GeV}\ \ (400\,\mathrm{GeV})\,. \tag{12}$$

   One stau candidate is required to fire the muon trigger 'in time',

$$\beta > 0.6\,. \tag{13}$$

2. Two stau candidates passing the muon chambers,

$$p_{\mathrm{T}}^{2\mu} > 150\,\mathrm{GeV}\ \ (360\,\mathrm{GeV})\,, \quad \beta^{\square} < 0.88\,, \tag{14}$$

   and

$$\beta > 0.6 \tag{15}$$

   for one stau.

3. Two stau candidates passing the tracker,

$$p_{\mathrm{T}}^{2\mu} > 300\,\mathrm{GeV}\ \ (500\,\mathrm{GeV})\,, \quad \beta^{\square} < 0.73\,, \tag{16}$$

   one of which has to pass the muon trigger chambers,

$$\beta_1 > \beta_{\mathrm{min}}^{\mathrm{tracker}}(m_{\tilde{\tau}_1})\,, \quad \beta_2 > \beta_{\mathrm{min}}^{\mathrm{trigger}}(m_{\tilde{\tau}_1})\,. \tag{17}$$

   This selection criterion assumes the modified trigger setup proposed in section 3.3.

Figure 4 shows the efficiencies of the selection criteria 1 to 3 for exemplary mass slices of the simplified models $\mathcal{A}$, $\mathcal{B}$ and $\mathcal{C}$. For all simplified models, selection criterion 1 is most efficient if the stau is sufficiently light. The large mass difference between LCP and stau ensures the production of high-p_{T} jets that enable a very good background rejection already in combination with the relatively loose velocity cut on β°, thus cutting away a smaller part of the signal than with the cut on $\beta^{\square}$. For heavier staus, high-p_{T} jets are no longer guaranteed. Consequently, selection criterion 2 becomes more efficient, relying on the cut on $\beta^{\square}$ to discriminate against muons with a mismeasured velocity. If the stau is very heavy, many events will contain slow staus that do not pass the cut $\beta > 0.6$. However, due to their large mass they have a very large p_{T}. Hence, selection criterion 3 is optimal for this part of the parameter space.

The background rejection obtained with these cuts is summarized in table 1 for the 8 TeV LHC. The relative importance of the background sources is similar for the 14 TeV run. The 14 TeV cuts provide a stronger background suppression as required by the larger integrated luminosity considered.

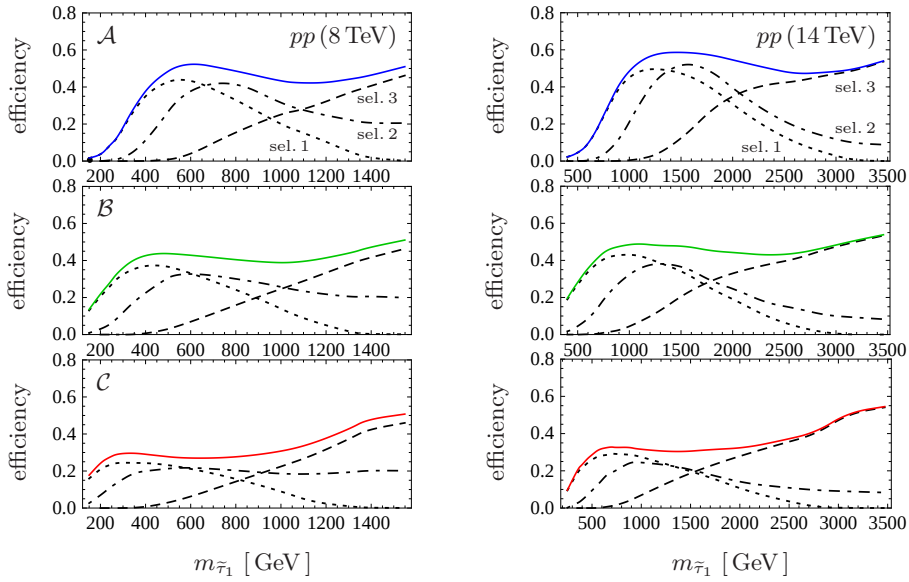

Figure 4: Efficiencies of the selection criteria 1 to 3 as functions of $m_{\tilde{\tau}_1}$ for fixed squark and gluino masses $m_{\tilde{g}} = m_{\tilde{q}} = 1600\,\text{GeV}$ (3600 GeV) for the 8 TeV (14 TeV) LHC and for the simplified models $\mathcal{A}$ (*top panels*), $\mathcal{B}$ (*middle*) and $\mathcal{C}$ (*bottom*). Trigger and reconstruction efficiencies are included. The solid curve denotes the union of all three cuts, i.e., the efficiency resulting from selecting all events satisfying at least one of the selection criteria.

4 Exploring the parameter space

4.1 Computation of the signal

To estimate the projected LHC reach for the simplified models described in section 2 we performed a full-fledged Monte Carlo study. Here we briefly sketch the computational steps of the analysis. The analysis was performed for the 8 TeV and 14 TeV LHC run. For the sake of saving computing time we factorized production and decay.

For the production we built up a grid of generator-level event files in the $m_{\tilde{g}}$-$m_{\tilde{q}}$ plane. We considered the production channels $\tilde{g}\tilde{g}$, $\tilde{g}\tilde{q}$, $\tilde{q}\tilde{q}$ and $\tilde{q}\bar{\tilde{q}}$ with a common squark mass for $\tilde{q} = \tilde{u}, \tilde{d}, \tilde{s}, \tilde{c}, \tilde{b}$. We computed the production cross sections for the different channels at NLO precision via Prospino 2 and simulated the events with the tree-level generator MadEvent 5. Since the size of NLO corrections differs significantly between the considered production channels, we performed a channel-wise normalization, i.e., we treated each production channel separately throughout the analysis chain. We generated a total of 30 000 events per mass point, apportioned between the four production channels according to their fraction of the total cross section. We used the CTEQ6L1 PDF set.

In a second step we passed the MadEvent events to Pythia 6 to perform the decay of the SUSY particles (and the showering and hadronization of SM particles). For each point on the $m_{\tilde{g}}$-$m_{\tilde{q}}$ grid, this allows for a variation of the spectrum below the LCP. We computed the decay widths and branching ratios (BR) via SDECAY [26]. The minimal

decay chain LCP $\to \widetilde{\chi}^0 \to \widetilde{\tau}$ was obtained by decoupling all other SUSY particles. The decay chain LCP $\to \widetilde{\chi}^0_2 \to \widetilde{\ell} \to \widetilde{\chi}^0_1 \to \widetilde{\tau}_1$ was enforced by computing the BR down to the $\widetilde{\chi}^0_2$ via SDECAY and adjusting the following BR accordingly.

The use of Pythia 6 for the decay of SUSY particles implies certain approximations whose validity we have to justify. Pythia 6 factorizes the cascade into decays of on-shell particles, using the narrow width approximation (i.e., each decay width is much smaller than the corresponding mass difference), and neglects spin correlations of fermions in the chain. Since we are interested in a systematic scan of the free parameters of the simplified models including regions where masses of sparticles in the decay chain are nearly mass degenerate, we have to ensure the validity of the use of factorization here.

The only kinematical cuts this analysis strongly relies on concern the β of the staus, the p_{T} of the staus and the p_{T} of the two hardest jets and combinations thereof. Consider the case where two SUSY particles in the cascade are very close in mass, i.e., their masses are much larger than the mass difference and much larger than the mass of the radiated SM particle. In this case the daughter sparticle basically inherits the kinematics of the mother sparticle and the SM particle appears as soft radiation. Its distribution might not be described well by the simulation. However, we do not cut on SM particles other than the jets. As the jets have to survive very severe p_{T} cuts, jets from such degenerate decays are very unlikely to contribute to our signal. We have explicitly checked the p_{T} distributions of the two hardest jets and the p_{T} and β distributions of the staus against a full matrix element simulation by Whizard [27] and found reasonably good agreement for different setups in which we considered the decay $\widetilde{q} \to q\widetilde{\chi}^0 \to q\tau\widetilde{\tau}_1$ for (nearly) degenerate $m_{\widetilde{q}}$ and $m_{\widetilde{\chi}^0}$, as well as nearly degenerate $m_{\widetilde{\chi}^0}$ and $m_{\widetilde{\tau}_1}$. The results differ by at most 10%. The resulting error on the efficiencies of the selection criteria which enters our final results is estimated to be even smaller, and is especially small compared to the dominant uncertainties, which are PDF and scale uncertainties that are introduced via the production cross section (for an error estimation see section 4.4). Thus, factorization is well-justified when relying on the considered observables.[11]

We included up to one additional jet in the matrix element. This introduces a source of potential double counting. Gluino-gluino production with an additional jet contains, for instance, a diagram with an intermediate squark. If the squark is on-shell, this contribution is equivalent to the lowest order gluino-squark production followed by the decay of the squark. To account for this, Prospino removes contributions from on-shell intermediate squarks and gluinos. Accordingly, we removed the same diagrams in the event generation in the course of the matching procedure in Pythia. As for the background, we applied the MLM matching procedure in order to match properly the jets from the matrix element and showering.

We passed the output of Pythia to the detector simulation Delphes 1.9. To account for long-lived staus we applied minor modifications on Delphes. The reconstruction efficiency for each stau was set to 0.9. We assumed a trigger efficiency of 90% [28].

[11] Relative angular distributions are affected more strongly by the applied approximation. Thus, larger deviations are present in ΔR. However, the dependence of our results on I_{rel} is very weak, as we stated in section 3.1. Consequently, the results are not affected noticeably.

4.2 LHC reach for a common squark mass

We estimate the LHC's sensitivity to observe or exclude the introduced simplified models as a function of the free parameters $m_{\widetilde{g}}$, $m_{\widetilde{q}}$ and $m_{\widetilde{\tau}_1}$. We consider a common squark mass $m_{\widetilde{q}}$ in this section. As discussed in section 2.1 the production is dominated by the first-generation squarks. Consequently, the derived limits can be interpreted as limits on the masses of these squarks. In section 4.3 we will consider the case of a light stop dominating the production cross section.

As shown in figure 4 the efficiencies of the selection criteria are typically about 0.5. On the other hand, as shown in table 1, the background expectation is reduced by these cuts to less than 10^{-2} events. Accordingly, a 95% C.L. exclusion[12] can always be claimed if no events are observed while three are expected. That is, the background rejection is saturated with these cuts. In such a situation the analysis is not very sensitive to the precise background cross section anymore (see e.g. [29]). Furthermore, discovery can also be claimed on the basis of very few events and the results for the exclusion curves represent an (typically even conservative) estimation of the 5σ discovery potential. These are typical features of the search for heavy stable charged sparticles.

Figures 5 and 6 show the resulting sensitivity for the 8 TeV and 14 TeV LHC run, respectively, for the three simplified models introduced in section 2.2. We visualize the variation of $m_{\widetilde{g}}$, $m_{\widetilde{q}}$ and $m_{\widetilde{\tau}_1}$ by showing slices of the parameter space. In the plots showing $m_{\widetilde{g}}$-$m_{\widetilde{\tau}_1}$ and $m_{\widetilde{q}}$-$m_{\widetilde{\tau}_1}$ planes, a fixed ratio $m_{\widetilde{q}}/m_{\widetilde{g}}$ is assumed. In the plots of the $m_{\widetilde{g}}$-$m_{\widetilde{q}}$ plane, we draw the sensitivity curves by conservatively choosing the stau mass that yields the smallest sensitivity at each point of the plane. In addition to strong production and decay, we include the production of staus by the direct DY process. In order to derive conservative limits we considered the stau mixing angle that yields the smallest cross section [29].[13] This contribution is always present and depends on the stau mass only.[14]

In model $\mathcal{A}$ (blue dashed lines) the decay LCP $\to \widetilde{\chi}^0$ leads to hard jets and potentially highly boosted staus. For moderate mass gaps $m_{\text{LCP}} - m_{\widetilde{\tau}_1}$ the staus are well-distinguishable from muons. The additional jet signature leads to a slight enhancement of the significance. For larger $m_{\text{LCP}} - m_{\widetilde{\tau}_1}$ a large number of staus are rejected by the velocity cut and the significance drops sharply, despite the fact that the jets become harder. This effect would hide the scenario very effectively from our selection criteria if it were not for the direct production, which increases the sensitivity for lower $m_{\widetilde{\tau}_1}$ (see figure 4, where we did not include the direct production). Thus, DY production allows us to cover the parameter space with a mostly model-independent search. Without it,

[12] We apply the CL_S method here.

[13] A significantly larger contribution of directly produced staus is possible, see e.g. [30].

[14] Similarly one could think of including the direct production of the intermediate sparticles that appear in the cascades. However, since there is no Drell-Yan production for pairs of pure binos the cross section can always be rendered negligible by an appropriate choice of the neutralino mixing. Hence, at least in the minimal decay chain, there is no such conservative minimal contribution. Including a minimal direct production cross section of the intermediate sparticles in longer decay chains would have a certain effect on the results in some of the considered regions in parameter space. However, this would run counter to the idea of this work.

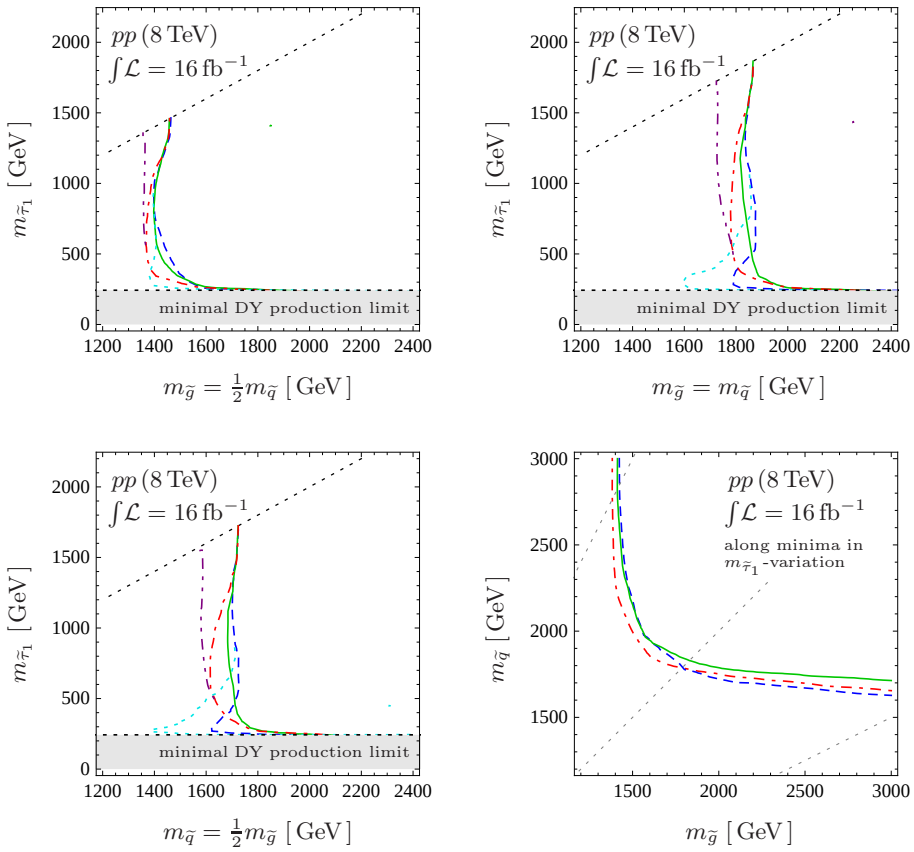

Figure 5: Projected LHC sensitivity (95% $\mathrm{CL_s}$ exclusion and approximate 5σ discovery reach, see text) for the models $\mathcal{A}$ (blue dashed), $\mathcal{B}$ (green solid) and $\mathcal{C}$ (red dot-dashed), as well as $\mathcal{A}$ (cyan dotted) and $\mathcal{C}$ (purple dot-dot-dashed) for a reduced set of selection criteria (see text for details). A common squark mass $m_{\tilde{q}}$ is assumed. In the lower right panel the curves represent the minima in the sensitivity with respect to the variation of $m_{\tilde{\tau}_1}$.

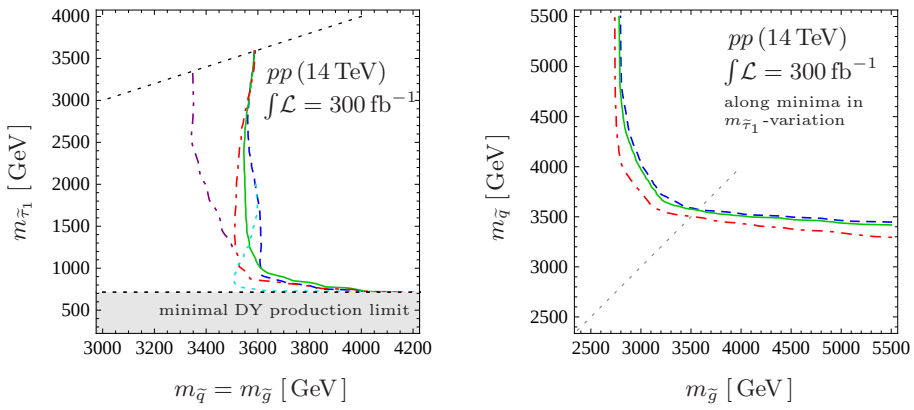

Figure 6: Projected LHC sensitivity (95% $\mathrm{CL_s}$ exclusion and approximate 5σ discovery reach, see text) for the models $\mathcal{A}$ (blue dashed), $\mathcal{B}$ (green solid) and $\mathcal{C}$ (red dot-dashed), as well as $\mathcal{A}$ (cyan dotted) and $\mathcal{C}$ (purple dot-dot-dashed) for a reduced set of selection criteria (see text for details). A common squark mass $m_{\tilde{q}}$ is assumed. In the right panel the curves represent the minima in the sensitivity with respect to the variation of $m_{\tilde{\tau}_1}$.

we were forced to introduce dedicated searches for each occurring topology to be able to cover the small $m_{\tilde{\tau}_1}$ region. For stau masses just above the region of dominant DY production (and for $m_{\tilde{g}} \gtrsim m_{\tilde{q}}$) the sensitivity for model $\mathcal{A}$ reaches a minimum (see upper right and lower left panel of figure 5). Higher luminosities push the corresponding mass reach up and cause the production to be closer to threshold. As a consequence, the minimum disappears in the projected sensitivity for the 14 TeV $300\,\mathrm{fb}^{-1}$ run (see left panel of figure 6). The cyan dotted curves show the sensitivity after dropping selection criterion 1, i.e., without taking the jet signature into account. The diminished sensitivity illustrates the importance of the additional jet signature in this region.

Model $\mathcal{C}$ has a sensitivity minimum in the intermediate range of $m_{\mathrm{LCP}} - m_{\tilde{\tau}_1}$. Many staus are rejected by the upper velocity cut in this region. Furthermore, compared to model $\mathcal{A}$ fewer hard jets are produced that could compensate for this effect.

As expected from the discussion in section 2.2, either $\mathcal{A}$ or $\mathcal{C}$ yields the minimal sensitivity for all values of $m_{\tilde{g}}$, $m_{\tilde{q}}$ and $m_{\tilde{\tau}_1}$. Model $\mathcal{B}$ behaves more moderately, resulting in a sensitivity in between those of the other models at most points.

For small mass gaps $m_{\mathrm{LCP}} - m_{\tilde{\tau}_1} \to 0$ all three models give the same efficiency. The mass pattern of the intermediate sparticles does not play a role in this regime. The staus basically inherit the velocity and angular distribution of the produced colored sparticles. In this parameter region lower limits on the velocity become important. As stated in section 3.3 current trigger restrictions cause the loss of events in which both staus have a velocity $\beta \lesssim 0.6$. For small mass gaps this loss is significant. This is illustrated by the purple dot-dot-dashed curves that show the sensitivity for model $\mathcal{C}$ after dropping selection criterion 3, which assumes buffering of the tracker data in order to be able to record several bunch crossings in delay. Especially for the 14 TeV run and $300\,\mathrm{fb}^{-1}$ luminosity, the implementation of such a trigger enhances the sensitivity significantly

(see left panel of figure 6).

In all the plots, the LHC sensitivities for the simplified models $\mathcal{A}$, $\mathcal{B}$ and $\mathcal{C}$ span a relatively narrow band although the mass patterns of the models are radically different. Furthermore, the overall dependence of the sensitivity on $m_{\widetilde{\tau}_1}$ is moderate. This situation is very different from the one in a missing E_{T} search like in neutralino LSP scenarios. There the sensitivity depends much more on the intermediate spectrum and on the mass of the LSP and it is more difficult to cover the limiting cases with appropriate simplified models. This shows that the simplified model approach is very suitable for the long-lived stau scenario. In the $m_{\widetilde{g}}$-$m_{\widetilde{q}}$ plane, where we took the most conservative choice for $m_{\widetilde{\tau}_1}$ at each point, the simplified models $\mathcal{A}$–$\mathcal{C}$ lie even more closely together. From the $m_{\widetilde{g}}$-$m_{\widetilde{q}}$ plane plots we can derive conservative projected limits on the gluino and squark masses in the common mass scenario. With $\int \mathcal{L} = 16\,\mathrm{fb}^{-1}$ at 8 TeV we expect gluino and squark masses of $m_{\widetilde{g}} \lesssim 1.4\,\mathrm{TeV}$ and $m_{\widetilde{q}} \lesssim 1.6\,\mathrm{TeV}$ to be either excluded or discovered. With $\int \mathcal{L} = 300\,\mathrm{fb}^{-1}$ at 14 TeV we are sensitive to $m_{\widetilde{g}} \lesssim 2.6\,\mathrm{TeV}$ and $m_{\widetilde{q}} \lesssim 3.3\,\mathrm{TeV}$. These limits allow for a completely model-independent interpretation with respect to all SUSY parameters that are not specified in this setup.

As already mentioned in section 2.2, asymmetric decay chains, i.e., one short and one long decay chain in one event, will also appear in realistic models. The selection criteria we imposed are not dedicated to such chains and asymmetric cascades will partly fail to be selected by these criteria. However, we expect that a dedicated extension of the selection criteria will provide equally high signal-to-background ratios. One could for instance require one very hard jet and an even stronger asymmetry in the stau kinematics.

Another aspect we noted in section 2.2 is the presence of heavy SM particle radiation in the 2-step decay LCP$\to \widetilde{\chi}_2^0 \to \widetilde{\chi}_1^0 \to \widetilde{\tau}$. To check whether threshold effects might affect the sensitivity significantly, we computed the corresponding curves for this 2-step decay. We explicitly allowed for the 3-body decay of the heavier neutralino into the lightest neutralino, which occurs once $m_{\widetilde{\chi}_2^0} - m_{\widetilde{\chi}_1^0} < m_Z$. The sensitivity curves for the 2-step decay lie completely between the 3-step decay (model $\mathcal{C}$) and the 1-step decay (model $\mathcal{B}$) in all plots of figures 5 and 6.

As another check of the generality of the introduced simplified models, we considered an inverted mass hierarchy in the simplified model $\mathcal{C}$, $m_{\widetilde{\ell}} < m_{\widetilde{\chi}^0}$. In this case a 3-body slepton decay occurs. In order to perform these computations we used an extension of the SDECAY package [31] allowing for the 3-body decays of sleptons. We found that for these spectra the picture drawn here does not change.

4.3 LHC reach for a light stop

As a complementary limit we will now consider the case of a light stop $\widetilde{t}_1$ and all other squarks decoupled. We set the gluino mass to $m_{\widetilde{g}} = 3m_{\widetilde{t}_1}$. In this setup processes other than stop-antistop production are negligible. Although the signature of the decaying stops might potentially provide a larger significance with a dedicated selection criterion, the benefit is expected to be marginal due to the high efficiencies that are already provided by the introduced cuts. Therefore, we refrain from introducing a dedicated selection here.

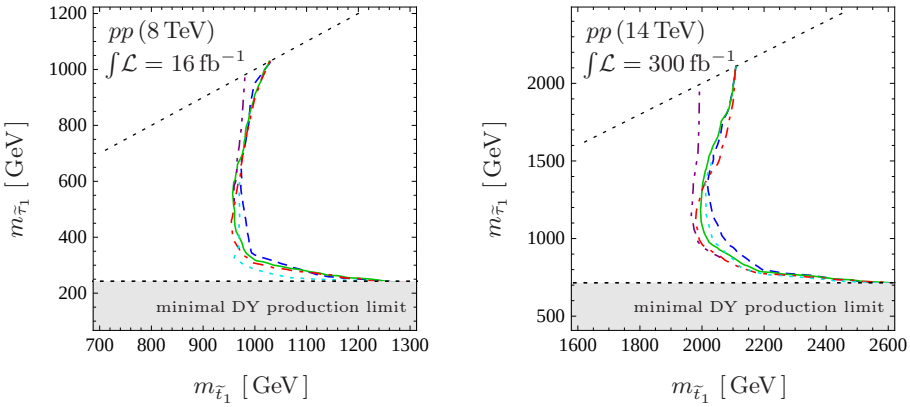

Figure 7: Projected LHC sensitivity (95% CL_s exclusion and approximate 5σ discovery reach, see section 4.2) for a light stop $\widetilde{t}_1$ and decoupled squarks and gluinos otherwise. As in figures 5 and 6 the lines denote the models $\mathcal{A}$ (blue dashed), $\mathcal{B}$ (green solid) and $\mathcal{C}$ (red dot-dashed), as well as $\mathcal{A}$ (cyan dotted) and $\mathcal{C}$ (purple dot-dot-dashed) for a reduced set of selection criteria (see section 4.2 for details).

Figure 7 shows the sensitivity in the $m_{\widetilde{t}_1}$-$m_{\widetilde{\tau}_1}$ plane. According to the lower production cross section for stops, the stop masses that are in reach of the LHC are smaller than the accessible squark masses that we have found in the common squark mass scenario considered in the previous section. The stau mass that is accessible via direct stau production is the same, of course. Correspondingly, the gap between the LCP mass and the lowest stau masses for which the production via cascades is dominant is considerably smaller. Therefore, the effect of the intermediate spectrum becomes less important and the curves for models $\mathcal{A}$–$\mathcal{C}$ lie even more closely together than in the previous section. In particular, the minimum of the sensitivity of model $\mathcal{A}$ just above the region of dominant direct DY production has disappeared. The velocity distribution of the staus varies less significantly with the stau mass in this scenario.

For $m_{\widetilde{t}_1} > m_{\widetilde{g}}$ we find the same sensitivity to $m_{\widetilde{g}}$ as in the large-$m_{\widetilde{q}}$ limit in the previous section. In conclusion, with $\int\mathcal{L} = 16\,\mathrm{fb}^{-1}$ at 8 TeV we expect gluino and stop masses of $m_{\widetilde{g}} \lesssim 1.4\,\mathrm{TeV}$ and $m_{\widetilde{t}_1} \lesssim 950\,\mathrm{GeV}$ to be either excluded or discovered. With $\int\mathcal{L} = 300\,\mathrm{fb}^{-1}$ at 14 TeV we are sensitive to $m_{\widetilde{g}} \lesssim 2.6\,\mathrm{TeV}$ and $m_{\widetilde{t}_1} \lesssim 2\,\mathrm{TeV}$.

4.4 Uncertainties

We shall briefly discuss the theoretical uncertainties of the cross section computations here. We expect these uncertainties to be the most important ones. Further uncertainties arise from the event generation and from the simplified detector simulation. We only consider the error implied by the scale dependence of the production cross section. The error introduced by PDF uncertainties is roughly of the same order. Uncertainties in the strong coupling α_s are expected to be somewhat smaller. A detailed discussion of the errors relevant for the production of colored sparticles at the LHC can be found in [32].

In the left panel of figure 8 we exemplarily show again the 8 TeV LHC sensitivity

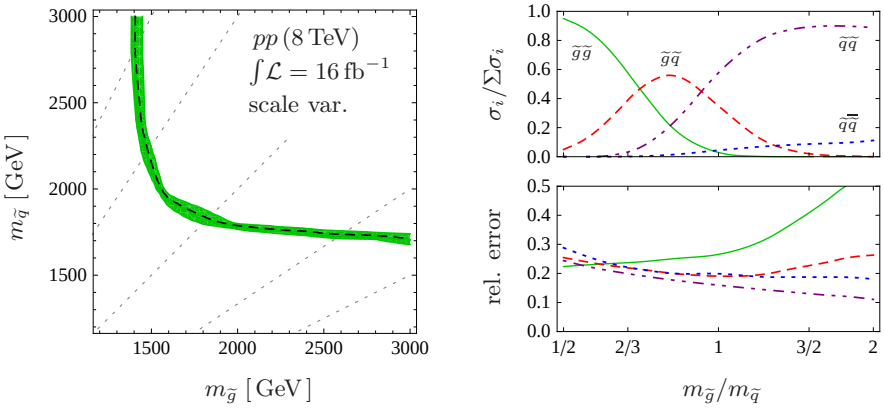

Figure 8: *Left:* LHC sensitivity in the $m_{\tilde{g}}$-$m_{\tilde{q}}$ plane for model $\mathcal{B}$ (black dashed curve, same as the green solid curve shown in the lower right panel of figure 5) and its error band according to the renormalization and factorization scale variation (green shaded region). *Upper right:* Fractional contributions of the considered production channels to the total production cross section of colored sparticles, parametrized by the ratio $m_{\tilde{g}}/m_{\tilde{q}}$, which is varied along the sensitivity limit shown in the left panel. *Lower right:* Relative errors in the cross sections due to scale variation for the considered production channels, again changing $m_{\tilde{g}}/m_{\tilde{q}}$ along the sensitivity limit.

for model $\mathcal{B}$ and a common squark mass (black dashed line). The green band shows the uncertainty implied by varying the scale in the range $m/2 \leq \mu \leq 2m$, where $\mu = \mu_\mathrm{F} = \mu_\mathrm{R}$ is the factorization and renormalization scale and m is the averaged mass of the produced sparticles. The error from scale dependence translates into uncertainties of roughly $\pm 20\,\mathrm{GeV}$ to $\pm 40\,\mathrm{GeV}$ in the squark and gluino masses. The lower right panel of figure 8 shows the relative error $|\sigma_{m/2} - \sigma_{2m}|/2\sigma_m$ of each production channel as a function of the ratio $m_{\tilde{g}}/m_{\tilde{q}}$, which is varied along the sensitivity limit shown in the left panel. The upper right panel of figure 8 shows the ratio of the respective cross section to the total cross section, again along the sensitivity curve. The average relative error is around 0.2 and is lowest in the region of a dominant $\widetilde{q}\widetilde{q}$ channel. The $\widetilde{g}\widetilde{g}$ production involves very large uncertainties for large $m_{\tilde{g}}/m_{\tilde{q}}$. However, in this region the cross section for $\widetilde{g}\widetilde{g}$ production is very small.

5 Stopped staus

So far we considered the signal of staus as heavy stable charged particles passing the detectors. As we already mentioned in section 3.3 very slow staus can lose their kinetic energy completely and get trapped inside the detector. These staus will then decay into the LSP inside the detector. This causes a signal that can be recorded with dedicated trigger algorithms [33, 34, 35]. The decay of the stau reveals very interesting information about the LSP and possibly even about the origin of SUSY breaking. Once the mass of

the stau is known[15] one can determine the LSP mass from reconstructed 2-body decays. Furthermore, for a gravitino LSP an unequivocal prediction of supergravity can be tested, namely the proportionality of the stau lifetime

$$\tau_{\tilde{\tau}} \simeq \frac{48\pi m_{3/2}^2 M_{\mathrm{P}}^2}{m_{\tilde{\tau}_1}^5} \left(1 - \frac{m_{3/2}^2}{m_{\tilde{\tau}_1}^2}\right)^{-4} \tag{18}$$

to the Planck mass squared [36, 37]. In scenarios with an axino LSP, stau decays may provide insights into the Peccei-Quinn sector [38].

In this section we will estimate the prospects for the LHC to observe decays of stopped staus by computing the number of staus that are expected to be stopped inside the detectors in the framework of our simplified models.[16] The mean range R of a charged particle (defined as the average thickness of absorber material the particle is capable of traversing) grows linearly with the particle's mass. Its dependence on $\gamma\beta$ is nearly linear in the double logarithmic plot [25] in the region of interest $\gamma\beta < 1$. In fact,

$$\log_{10}\left(\frac{R/\mathrm{g\,cm^{-2}}}{m/\mathrm{GeV}}\right) = c_1 + c_2 \log_{10}(\gamma\beta) \tag{19}$$

approximates $R(\gamma\beta)$ to a precision better than 1%. For iron $c_1 \simeq 2.16$ and $c_2 \simeq 3.32$. From (19) we determine the maximal velocity of a stau with mass $m_{\tilde{\tau}_1}$ to be expected to stop inside the detector, $\beta^R_{\mathrm{max}}(m_{\tilde{\tau}_1})$. Conservatively, we assume a maximal range of $R_{\mathrm{max}} = 2400\,\mathrm{g\,cm^{-2}}$. This is a conservative estimation of the thickness of a CMS-like detector in the central region.[17]

Figure 9 shows the expected number of events that provide at least one stau which is expected to stop inside the detector, i.e., with $\beta < \beta^R_{\mathrm{max}}(m_{\tilde{\tau}_1})$. According to the discussion in section 2.2, for large mass gaps $m_{\mathrm{LCP}} - m_{\tilde{\tau}_1}$ staus are expected to be considerably slower in model $\mathcal{C}$ than in model $\mathcal{A}$. As a consequence, the numbers of stopped staus typically differ by an order of magnitude.

At the 8 TeV LHC only a few stopping events are expected in the mass region of interest. Thus, most likely it will not be possible to study the properties of stau decays in detail. The high-luminosity 14 TeV run, however, will provide reasonable numbers of stopped staus in scenarios that lie within the discovery reach of the full 8 TeV dataset or the early 14 TeV dataset. Consequently, such scenarios are expected to be accessible in sufficient detail to determine the stau lifetime. Determining the LSP mass seems feasible as well, unless $m_{\mathrm{LSP}} \lesssim 0.1\, m_{\tilde{\tau}_1}$, in which case the mass determination becomes extremely difficult because it requires a very precise measurement of the tau recoil energy.

[15] The mass is determined already at the stage of discovery by measuring the momentum and the velocity [21, 22].

[16] Since a detailed study of the LHC's potential for measuring the stau lifetime and LSP mass requires a precise detector simulation taking into account details of the LHC operating schedule, we leave this to the experimental collaborations. Combining our results with those of [34] it may be possible to estimate the prospects for measuring the lifetime in the simplified models.

[17] We took into account 20 layers of silicon ($2.33\,\mathrm{g/cm^3}$), each 0.5 mm thick; 1 layer of ECAL crystal ($8.28\,\mathrm{g/cm^3}$), 23 cm thick; 16 layers of HCAL brass ($8.53\,\mathrm{g/cm^3}$), each around 6 cm thick; 1 magnet of NbTi ($5.6\,\mathrm{g/cm^3}$), 31.2 cm thick; 3 layers of iron yokes ($7.87\,\mathrm{g/cm^3}$), 30, 63 and 63 cm thick [39].

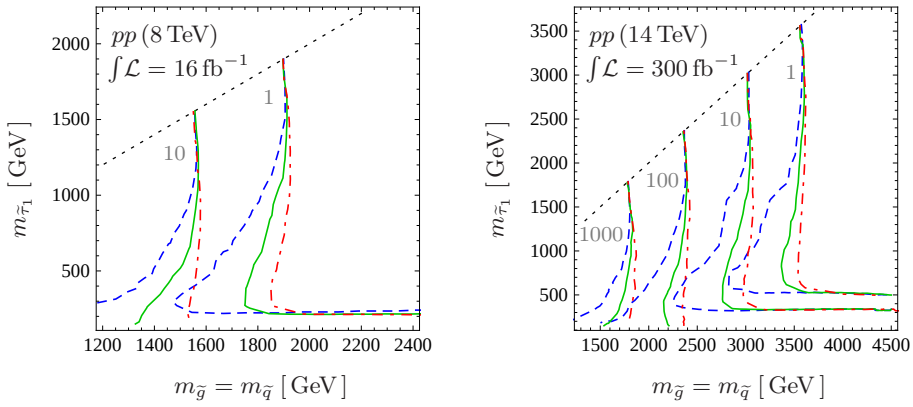

Figure 9: Number of events that contain at least one stau which is stopped inside the detector for the simplified models $\mathcal{A}$ (blue dashed), $\mathcal{B}$ (green solid) and $\mathcal{C}$ (red dot-dashed). The iso-event-number curves are displayed in the $m_{\tilde{g}}$-$m_{\tilde{\tau}_1}$ plane where we have chosen the common squark mass scenario and $m_{\tilde{q}} = m_{\tilde{g}}$.

A more detailed study of stau decays including the measurement of the spin of the LSP via reconstructed 3-body decays [36, 38] may only be possible at an e^+e^- collider with a dedicated detector environment, see e.g. [40, 41, 42, 43].

6 Conclusions

We have studied the potential of the LHC to discover or exclude scenarios with a long-lived stau (or another charged slepton) in a simplified-model approach. The production of colored sparticles is likely to be the dominant production mode at the LHC. SUSY events are characterized by muon-like particles that leave the detector and can be slow. In addition, hard jets can be expected in some cases. We have defined 2×3 discrete simplified models covering the limiting cases concerning the production and the decay, respectively. Each model contains only three free parameters, $m_{\tilde{\tau}_1}$, $m_{\tilde{g}}$ and either the common squark mass $m_{\tilde{q}}$ or $m_{\tilde{t}_1}$. We have also included the Drell-Yan production of stau pairs.

Due to the very prominent signature of long-lived staus, exclusion and discovery take place on the basis of a very few events. Consequently, a discovery could be established in a rather short period of time. Due to the direct DY contribution, regions where both staus are typically too fast to be identified (where SM particle radiation would provide a more significant signal) are not present. For the same reason, no very specific cuts are required, enabling a model-independent analysis. In other words, it is possible to cover the whole parameter space with a small number of selection criteria that yield both a high signal efficiency and a very good background rejection. In almost the whole parameter space, we have found a signal efficiency around 50%. Even in the most challenging region, the efficiency does not drop below roughly 20%. This shows that in the long-lived stau

scenario no regions exist where the theory effectively hides from observation. This is a striking difference to the neutralino LSP scenario, where both compressed spectra and very stretched ones are very hard to observe.

If all squarks have a common mass the most conservative projected limits for $\int \mathcal{L} = 16\,\text{fb}^{-1}$ at the 8 TeV LHC ($\int \mathcal{L} = 300\,\text{fb}^{-1}$ at 14 TeV) are $m_{\tilde{q}} \gtrsim 1.6\,\text{TeV}$ ($m_{\tilde{q}} \gtrsim 3.3\,\text{TeV}$). If a stop is significantly lighter than the other squarks the corresponding limits become $m_{\tilde{t}_1} \gtrsim 950\,\text{GeV}$ ($m_{\tilde{t}_1} \gtrsim 2\,\text{TeV}$). In both cases the gluino is expected to be either excluded or discovered up to a mass of $m_{\tilde{g}} \simeq 1.4\,\text{TeV}$ ($m_{\tilde{g}} \simeq 2.6\,\text{TeV}$). Intermediate cases may be estimated by interpolating the results according to the discussion in section 2.1. Already the data collected so far should allow one to place lower limits above a TeV on both $m_{\tilde{q}}$ and $m_{\tilde{g}}$ even in the most challenging scenario. The actual experimental searches might achieve even better sensitivities, since we chose quite conservative assumptions concerning background rejection and detector efficiencies.

Staus stopped in the detectors could provide intriguing possibilities to test supergravity or to gain insights into the SUSY breaking mechanism. We have computed the number of stopped stau events in the framework of the simplified models. Especially for very compressed spectra, the LHC provides a very good environment to measure the stau lifetime.

Acknowledgements

We would like to thank Sergei Bobrovskyi, Jim Brooke, Silja Brensing, Giacomo Bruno, Jie Chen, James Hirschauer, Kolja Kaschube, Tomas Kasemets, Boris Panes, Loic Quertenmont, Peter Schleper and Daniel Wiesler for very helpful discussions. Very special thanks go to Dao Thi Nhung and Sabine Kraml for generously providing their SDECAY extension for three-body lepton decays. This work was supported by the German Science Foundation (DFG) via the Junior Research Group 'SUSY Phenomenology' within the Collaborative Research Center 676 'Particles, Strings and the Early Universe'.

References

[1] MSSM Working Group, A. Djouadi *et al.*, "The Minimal Supersymmetric Standard Model: Group Summary Report", `arXiv:hep-ph/9901246`.

[2] C. F. Berger, J. S. Gainer, J. L. Hewett, and T. G. Rizzo, "Supersymmetry Without Prejudice", *JHEP* **0902** (2009) 023, `arXiv:0812.0980 [hep-ph]`.

[3] J. Alwall, P. Schuster, and N. Toro, "Simplified Models for a First Characterization of New Physics at the LHC", *Phys. Rev.* **D79** (2009) 075020, `arXiv:0810.3921 [hep-ph]`.

[4] LHC New Physics Working Group, D. Alves *et al.*, "Simplified Models for LHC New Physics Searches", `arXiv:1105.2838 [hep-ph]`.

[5] W. Beenakker, R. Höpker, M. Spira, and P. Zerwas, "Squark and gluino production at hadron colliders", *Nucl. Phys.* **B492** (1997) 51–103, arXiv:hep-ph/9610490. http://www.thphys.uni-heidelberg.de/~plehn/index.php?show=prospino.

[6] P. Konar, K. T. Matchev, M. Park, and G. K. Sarangi, "How to look for supersymmetry under the lamppost at the LHC", *Phys. Rev. Lett.* **105** (2010) 221801, arXiv:1008.2483 [hep-ph].

[7] C. Horn, "A Bottom-Up Approach to SUSY Analyses", *J. Phys.* **G36** (2009) 105005, arXiv:0905.4497 [hep-ex].

[8] R. Gavin, Y. Li, F. Petriello, and S. Quackenbush, "FEWZ 2.0: A code for hadronic Z production at next-to-next-to-leading order", *Comput. Phys. Commun.* **182** (2011) 2388–2403, arXiv:1011.3540 [hep-ph]. http://gate.hep.anl.gov/fpetriello/FEWZ.html.

[9] J. M. Campbell, R. Ellis, and C. Williams, "Vector boson pair production at the LHC", *JHEP* **1107** (2011) 018, arXiv:1105.0020 [hep-ph].

[10] J. M. Campbell, R. K. Ellis, and F. Tramontano, "Single top production and decay at next-to-leading order", *Phys. Rev.* **D70** (2004) 094012, arXiv:hep-ph/0408158.

[11] J. M. Campbell and F. Tramontano, "Next-to-leading order corrections to W t production and decay", *Nucl. Phys.* **B726** (2005) 109–130, arXiv:hep-ph/0506289.

[12] J. M. Campbell, R. K. Ellis, F. Febres Cordero, F. Maltoni, L. Reina, D. Wackeroth, and S. Willenbrock, "Associated production of a W boson and one b jet", *Phys. Rev.* **D79** (2009) 034023, arXiv:0809.3003 [hep-ph].

[13] J. Campbell, F. Caola, F. Febres Cordero, L. Reina, and D. Wackeroth, "NLO QCD predictions for $W + 1$ jet and $W + 2$ jet production with at least one b jet at the 7 TeV LHC", *Phys.Rev.* **D86** (2012) 034021, arXiv:1107.3714 [hep-ph].

[14] J. M. Campbell and R. Ellis, *MCFM – Monte Carlo for FeMtobarn processes.* http://mcfm.fnal.gov/.

[15] J. Alwall, M. Herquet, F. Maltoni, O. Mattelaer, and T. Stelzer, "MadGraph 5: Going Beyond", *JHEP* **1106** (2011) 128, arXiv:1106.0522 [hep-ph].

[16] T. Sjöstrand, S. Mrenna, and P. Skands, "PYTHIA 6.4 physics and manual", *JHEP* **0605** (2006) 026, arXiv:hep-ph/0603175.

[17] J. Alwall, S. Höche, F. Krauss, N. Lavesson, L. Lönnblad, F. Maltoni, M. L. Mangano, M. Moretti, C. G. Papadopoulos, F. Piccinini, S. Schumann, M. Treccani, J. Winter, and M. Worek, "Comparative study of various algorithms for the merging of parton showers and matrix elements in hadronic collisions", *Eur. Phys. J.* **C53** (2008) 473–500, arXiv:0706.2569 [hep-ph].

[18] J. Pumplin, D. R. Stump, J. Huston, H. L. Lai, P. Nadolsky, and W. K. Tung, "New generation of parton distributions with uncertainties from global QCD analysis", *JHEP* **0207** (2002) 012, arXiv:hep-ph/0201195.

[19] S. Ovyn, X. Rouby, and V. Lemaitre, "DELPHES, a framework for fast simulation of a generic collider experiment", arXiv:0903.2225 [hep-ph]. http://www.fynu.ucl.ac.be/users/s.ovyn/Delphes/download.html.

[20] M. Cacciari, G. P. Salam, and G. Soyez, "The anti-k_t jet clustering algorithm", *JHEP* **0804** (2008) 063, arXiv:0802.1189 [hep-ph].

[21] ATLAS Collaboration, G. Aad *et al.*, "Search for heavy long-lived charged particles with the ATLAS detector in pp collisions at $\sqrt{s} = 7$ TeV", *Phys. Lett.* **B703** (2011) 428–446, arXiv:1106.4495 [hep-ex].

[22] CMS Collaboration, "Search for Heavy Stable Charged Particles", CMS-PAS-EXO-11-022, CERN, Geneva, Jul, 2011. http://cds.cern.ch/record/1370057.

[23] CMS Collaboration, "Search for Heavy Stable Charged Particles in pp collisions at $\sqrt{s} = 7$ TeV", CMS-PAS-EXO-10-004, CERN, Geneva, Jul, 2010. http://cds.cern.ch/record/1280690.

[24] CMS Collaboration, "Search for heavy stable charged particles with 100 pb^{-1} and 1 fb^{-1} in the CMS experiment", CMS-PAS-EXO-08-003, CERN, Geneva, Feb, 2009. http://cdsweb.cern.ch/record/1152570.

[25] Particle Data Group, K. Nakamura *et al.*, "Review of particle physics", *J. Phys.* **G37** (2010) 075021.

[26] M. Mühlleitner, A. Djouadi, and Y. Mambrini, "SDECAY: A Fortran code for the decays of the supersymmetric particles in the MSSM", *Comput. Phys. Commun.* **168** (2005) 46–70, arXiv:hep-ph/0311167.

[27] W. Kilian, T. Ohl, and J. Reuter, "WHIZARD: Simulating Multi-Particle Processes at LHC and ILC", *Eur. Phys. J.* **C71** (2011) 1742, arXiv:0708.4233 [hep-ph]. http://projects.hepforge.org/whizard/.

[28] K. Kaschube, *Search for Stable Stau Production at the LHC*. PhD thesis, University of Hamburg, 2011. http://inspirehep.net/record/940823.

[29] J. Heisig and J. Kersten, "Production of long-lived staus in the Drell-Yan process", *Phys. Rev.* **D84** (2011) 115009, arXiv:1106.0764 [hep-ph].

[30] J. M. Lindert, F. D. Steffen, and M. K. Trenkel, "Direct stau production at hadron colliders in cosmologically motivated scenarios", *JHEP* **1108** (2011) 151, arXiv:1106.4005 [hep-ph].

[31] S. Kraml and D. Nhung, "Three-body decays of sleptons in models with non-universal Higgs masses", *JHEP* **0802** (2008) 061, arXiv:0712.1986 [hep-ph].

[32] W. Beenakker, S. Brensing, M. Krämer, A. Kulesza, E. Laenen, *et al.*, "Squark and gluino hadroproduction", *Int. J. Mod. Phys.* **A26** (2011) 2637–2664, arXiv:1105.1110 [hep-ph].

[33] S. Asai, K. Hamaguchi, and S. Shirai, "Measuring lifetimes of long-lived charged massive particles stopped in LHC detectors", *Phys. Rev. Lett.* **103** (2009) 141803, arXiv:0902.3754 [hep-ph].

[34] J. Pinfold and L. Sibley, "Measuring the Lifetime of Trapped Sleptons Using the General Purpose LHC Detectors", *Phys. Rev.* **D83** (2011) 035021, arXiv:1006.3293 [hep-ph].

[35] P. W. Graham, K. Howe, S. Rajendran, and D. Stolarski, "New Measurements with Stopped Particles at the LHC", *Phys. Rev.* **D86** (2012) 034020, arXiv:1111.4176 [hep-ph].

[36] W. Buchmüller, K. Hamaguchi, M. Ratz, and T. Yanagida, "Supergravity at colliders", *Phys. Lett.* **B588** (2004) 90–98, arXiv:hep-ph/0402179.

[37] J. L. Feng, A. Rajaraman, and F. Takayama, "Probing gravitational interactions of elementary particles", *Int. J. Mod. Phys.* **D13** (2004) 2355–2359, arXiv:hep-th/0405248.

[38] A. Brandenburg, L. Covi, K. Hamaguchi, L. Roszkowski, and F. D. Steffen, "Signatures of axinos and gravitinos at colliders", *Phys. Lett.* **B617** (2005) 99–111, arXiv:hep-ph/0501287.

[39] CMS Collaboration, S. Chatrchyan *et al.*, "The CMS experiment at the CERN LHC", *JINST* **3** (2008) S08004.

[40] K. Hamaguchi, Y. Kuno, T. Nakaya, and M. M. Nojiri, "A Study of late decaying charged particles at future colliders", *Phys. Rev.* **D70** (2004) 115007, arXiv:hep-ph/0409248.

[41] J. L. Feng and B. T. Smith, "Slepton trapping at the large hadron and international linear colliders", *Phys. Rev.* **D71** (2005) 015004, arXiv:hep-ph/0409278.

[42] H.-U. Martyn, "Detecting metastable staus and gravitinos at the ILC", *Eur. Phys. J.* **C48** (2006) 15–24, arXiv:hep-ph/0605257.

[43] O. Çakır, İ. T. Çakır, J. R. Ellis, and Z. Kırca, "Study of Metastable Staus at Linear Colliders", arXiv:hep-ph/0703121.